Phase composition of calcium phosphate materials affects bone formation by modulating osteoclastogenesis

Paul Humbert, Carina Kampleitner, Julien de Lima, Meadhbh Á Brennan, Irene Lodoso-Torrecilla, Joanna Maria Sadowska, Frédéric Blanchard, Cristina Canal, Maria-Pau Ginebra, Oskar Hoffmann, et al.

Acta Biomaterialia 176 (2024) 417–431

Contents lists available at ScienceDirect

Acta Biomaterialia

journal homepage: www.elsevier.com/locate/actbio

Full length article

Phase composition of calcium phosphate materials affects bone formation by modulating osteoclastogenesis

Paul Humbert[a,b,1], Carina Kampleitner[c,d,e,f,1], Julien De Lima[a,b], Meadhbh Á Brennan[g], Irene Lodoso-Torrecilla[h,i], Joanna Maria Sadowska[h,i], Frédéric Blanchard[a,b], Cristina Canal[h,i], Maria-Pau Ginebra[h,i,j], Oskar Hoffmann[d,1], Pierre Layrolle[a,k,1,*]

[a] INSERM, UMR 1238, Phy-OS, Bone Sarcoma and Remodeling of Calcified Tissues, School of Medicine, University of Nantes, Nantes, France
[b] INSERM, UMR 1229, RMeS, Regenerative Medicine and Skeleton, University of Nantes, Oniris, CHU Nantes, Nantes, France
[c] Karl Donath Laboratory for Hard Tissue and Biomaterial Research, University Clinic of Dentistry, Medical University of Vienna, Vienna, Austria
[d] Division of Pharmacology and Toxicology, Department of Pharmaceutical Sciences, University of Vienna, Vienna, Austria
[e] Ludwig Boltzmann Institute for Traumatology, The Research Center in Cooperation With AUVA, Vienna, Austria
[f] Austrian Cluster of Tissue Regeneration, Vienna, Austria
[g] Regenerative Medicine Institute, School of Medicine and Biomedical Engineering, School of Engineering, University of Galway, Galway, Ireland
[h] Biomaterials, Biomechanics and Tissue Engineering Group, Department of Materials Science and Engineering, Universitat Politècnica de Catalunya, Barcelona, Spain
[i] Research Centre in Multiscale Science and Engineering, Universitat Politècnica de Catalunya, Barcelona, Spain
[j] Institute of Bioengineering of Catalonia, Barcelona Institute of Science and Technology, Barcelona, Spain
[k] INSERM, UMR 1214, ToNIC, CHU Purpan, Université Paul Sabatier, Toulouse, France

ARTICLE INFO

Article history:
Received 10 October 2023
Revised 12 January 2024
Accepted 17 January 2024
Available online 23 January 2024

Keywords:
Calcium phosphates
Osteoclasts
Bone formation
Human mesenchymal stromal cells
Material composition

ABSTRACT

Human mesenchymal stromal cells (hMSCs) seeded on calcium phosphate (CaP) bioceramics are extensively explored in bone tissue engineering and have recently shown effective clinical outcomes. In previous pre-clinical studies, hMSCs-CaP-mediated bone formation was preceded by osteoclastogenesis at the implantation site. The current study evaluates to what extent phase composition of CaPs affects the osteoclast response and ultimately influence bone formation. To this end, four different CaP bioceramics were used, hydroxyapatite (HA), β-tricalcium phosphate (β-TCP) and two biphasic composites of HA/β-TCP ratios of 60/40 and 20/80 respectively, for *in vitro* osteoclast differentiation and correlation with *in vivo* osteoclastogenesis and bone formation. All ceramics allowed osteoclast formation *in vitro* from mouse and human precursors, except for pure HA, which significantly impaired their maturation. Ectopic implantation alongside hMSCs in subcutis sites of nude mice revealed new bone formation at 8 weeks in all conditions with relative amounts for β-TCP > biphasic CaPs > HA. Surprisingly, while hMSCs were essential for osteoinduction, their survival did not correlate with bone formation. By contrast, the degree of early osteoclastogenesis (2 weeks) seemed to define the extent of subsequent bone formation. Together, our findings suggest that the osteoclastic response could be used as a predictive marker in hMSC-CaP-based bone regeneration and strengthens the need to understand the underlying mechanisms for future biomaterial development.

Statement of significance

The combination of mesenchymal stromal cells (MSCs) and calcium phosphate (CaP) materials has demonstrated its safety and efficacy for bone regeneration in clinical trials, despite our insufficient understanding of the underlying biological mechanisms. Osteoclasts were previously suggested as key mediators between the early inflammatory phase following biomaterial implantation and the subsequent bone formation. Here we compared the affinity of osteoclasts for various CaP materials with different ratios

* Corresponding author.
E-mail address: pierre.layrolle@inserm.fr (P. Layrolle).
[1] These authors contributed equally.

https://doi.org/10.1016/j.actbio.2024.01.022

of hydroxyapatite to β-tricalcium phosphate. We found that osteoclast formation, both in vitro and at early stages in vivo, correlates with bone formation when the materials were implanted alongside MSCs in mice. Surprisingly, MSC survival did not correlate with bone formation, suggesting that the number or phenotype of osteoclasts formed was more important.

Introduction

Autologous bone grafting is the method of choice in treating non-union fractures and other large skeletal defects caused by trauma, cancer or metabolic diseases [1,2] but it is associated with drawbacks such as limited availability, donor site morbidity and rapid resorption. In recent years, this gold standard has been challenged by innovative therapies relying on the combination of osteoconductive biomaterials with osteogenic factors or stem cells [3,4]. Among the most promising strategies, the combination of biphasic calcium phosphate (BCP) bioceramics and mesenchymal stromal cells (MSCs) culture expanded from the bone marrow, has proven its safety and efficacy in treating long bone non-unions or maxillofacial defects in patients [5–7]. Despite these clinical achievements, the exact mechanisms leading to bone regeneration remain unclear and its understanding is necessary in order to develop or select optimal delivery biomaterials. It was widely believed that the therapeutic value of MSCs for bone repair is based on their ability to differentiate into different cell types. However, several studies have revealed that the vast portion of donor MSCs dies shortly after implantation due to lack of oxygen and glucose, and that the newly formed bone is primarily of host origin [8–11].

Osteoclasts are well recognized for their role as bone-resorbing cells. During bone healing, osteoclasts participate in a well-orchestrated process together with several other cell types to restore the skeletal function [12]. During the early stage of bone healing, i.e., inflammatory phase, osteoclasts resorb dead and necrotic bone at the injury site, while later on, they are active in the remodeling process [13]. Osteoclasts also communicate with bone-forming cells derived from MSCs to coordinate new bone deposition. These messages can be sent by various means: bone matrix-released growth factors, osteoclast-secreted proteins (clastokines), extracellular vesicles, and membrane-bound factors. These coupling factors can either stimulate or inhibit osteoblast differentiation and bone formation [14].

In the context of bone tissue engineering, calcium phosphates (CaP) are particularly interesting due to their biocompatibility, biodegradability, osteoconductivity, and chemical similarity to the mineral phase of bone [15,16]. They are usually obtained by sintering at high temperatures which generates hydroxyapatite (HA) and β-tricalcium phosphate (β-TCP) bioceramics having different phase composition, solubility in body fluids, micro-, macro- porosity and specific surface area [17]. When CaP materials are implanted in an extra-osseous site, such as muscle or subcutis, osteoclasts show an early appearance before new bone is formed. Further, their recruitment to the implantation site is significantly enhanced, when CaP were pre-loaded with MSCs [9,18]. Interestingly, inhibiting the early osteoclastic response via an anti-RANKL-antibody or an anti-osteoporotic drug (e.g., clodronate) impaired subsequent bone formation *in vivo* [9,19], highlighting the pivotal role of osteoclasts in bone formation in this context.

Bioceramics made of HA, β-TCP, or mixtures of both (biphasic calcium phosphate, BCP) have been extensively investigated for bone regeneration [17]. Most clinical applications use BCP with the HA/β-TCP ratio of 20/80 based on the outcome of subcutaneous implantation experiments in mice [8]. However, this composition did not perform drastically better than other formulations when associated with hMSCs [20]. The bioactivity of BCP occurs through the chemical dissolution in body fluids of the most soluble phase β-TCP and the reprecipitation of biological apatite on the stable HA while their cellular resorption by foreign body giant cells and in some cases, osteoclasts remain limited. Nevertheless, osteoclasts' adhesion, differentiation, and activity can be influenced by material-specific parameters such as chemical composition, surface roughness, dissolution rate, grain size or microporosity [21–26]. Physicochemical properties do not only affect osteoclast development and activity, but they can also modulate the crosstalk between osteoclasts and bone-forming osteoblasts. Shiwaku et al. reported that an increasing percentage of HA in BCP reduced *in vitro* osteoclastogenesis and the expression and secretion of positive coupling factors that in turn modulate osteoblast function [27].

Given these data, the main objective of this manuscript was to demonstrate whether phase composition of CaPs can affect osteoclastogenesis, both *in vitro* and *in vivo*. We tested this hypothesis using four CaP formulations with various proportions of HA and β-TCP: pure HA, pure β-TCP and BCPs with HA/β-TCP ratios of 60/40 and 20/80. We evaluated the ability of these materials to support osteoclastogenesis *in vitro*, using human and mouse precursors. Then, we correlated these observations with *in vivo* responses in a subcutaneous nude mouse model to study the relationship between the level of osteoclastogenesis and newly formed bone. In the ectopic site, hMSCs were transplanted alongside the CaP materials to create an osteoinductive environment with subsequent analysis of their engraftment and survival.

2. Materials and methods

2.1. Biomaterials and bone slices

2.1.1. Preparation of CaP discs and granules

Discs were prepared through a cement reaction using a solid phase consisting of 98 wt. % α- α-tricalcium phosphate (α-TCP) and 2 wt. % precipitated hydroxyapatite (PHA, Merck, Germany) mixed with water at a liquid-to-powder ratio of 0.65 mL/g. The synthesis of α-TCP was performed as previously described in Ginebra et al. [28]. Briefly, α-TCP was prepared by heating calcium hydrogen phosphate ($CaHPO_4$, Sigma-Aldrich, USA) and calcium carbonate ($CaCO_3$, Sigma-Aldrich) in a molar ratio of 2:1 at 1400°C for 15 h, followed by quenching in air. α-TCP powder (5.2 µm median size) was obtained by milling in an agate ball mill (Pulverisette 6, Fritsch GmbH, Germany) with 10 balls (d = 30 mm) for 15 min at 450 rpm. The cement paste was placed in Teflon molds of 2 mm in height and 6 mm in diameter and left in a humid atmosphere at 37°C for 7 hours to achieve cohesion. From here, two different routes were followed: I) for β-TCP discs, the samples were immersed in water at 37°C for 10 days to allow for complete hydrolysis to calcium-deficient hydroxyapatite and were subsequently sintered at 1100°C for 15 h; II) for BCP discs in a 20/80 and 60/40 HA:β-TCP ratio and for stoichiometric HA discs, a previously developed protocol was used [29]. Briefly, the samples were immersed in a 0.01 wt. %, 0.45 wt. % or 2 wt. % sodium bicarbonate ($NaHCO_3$, Sigma-Aldrich) solution for BCP 20/80, BCP 60/40 and HA respectively, and a hydrothermal treatment was applied by autoclaving at

121°C and 1 bar for 30 minutes. Subsequently, samples were thoroughly washed with deionized water and sintered at 1100°C for 15 h. To obtain granules, the discs were manually milled and sieved between 590 and 840 µm (mean particle size 770 ± 130 µm).

For *in vitro* testing, discs were sterilized with 70 % ethanol for 30 min, followed by three washing cycles with phosphate-buffered saline (PBS, Gibco, Thermo Fisher Scientific, USA) prior to preincubating them in complete culture media containing alpha-minimum essential medium (αMEM; Gibco, Thermo Fisher Scientific), 10 % fetal bovine serum, 100 U/ml penicillin and 100 μg/ml streptomycin (Eurobio, France; Biochrom, Germany) for 24 h at 37°C and 5 % CO_2. Granular material for subcutaneous implantation was sterilized by gamma-irradiation (23.5 kGy) and pre-incubated in serum-free αMEM for 24 h under classical cell culture conditions (37°C, 5 % CO_2).

2.1.2. Material characterization

The phase composition of CaP biomaterials was analyzed by X-ray diffraction using a diffractometer (D8 Advance, Bruker Corp., USA) equipped with a Cu Kα anode operated at 40 kV and 40 mA. Data were collected in 0.02° steps over the 2θ range of 20°–40° with a counting time of 2 s per step. Phase identification was accomplished by comparing the experimental patterns to those of HA (JCPDS 86-1201), and β-TCP (JCPDS 70-2065). Semiquantitative phase-composition analyses were carried out using DIFFRAC.EVA software (Bruker, USA). The skeletal density was measured by helium pycnometry (AccuPyc 133; Micromeritics, USA). The specific surface area was determined by nitrogen adsorption using the BET (Brunauer-Emmett-Teller) method (Gemini VII, Micromeritics) and the open porosity and pore entrance size distributions were obtained by mercury intrusion porosimetry (MIP, Autopore IV Micromeritics).

The ultrastructure of CaP discs was visualized using scanning electron microscopy (SEM). Briefly, discs were placed on a sample holder and imaged without any sample preparation at 5 kV with a TM3000 Tabletop SEM (Hitachi, Japan).

2.1.3. Preparation of bovine bone slices

Bovine cortical bone discs were prepared as described in Kampleitner et al. [30]. Briefly, dried bovine cortical bone was cut into 300-350 µm thick slices using a low-speed diamond saw (Buehler, USA). These bone slices were further punched into round discs (Ø = 5 mm) and subsequently washed with distilled water, 70 % and 100 % ethanol in an ultrasonic bath. After that, bone slices were irradiated with UV light for 15 min on each side under sterile conditions. For *in vitro* testing, bone discs were preincubated in complete culture media for 24 h.

2.1.4. In vitro *calcium release and adsorption by CaP discs and bone slices*

To investigate ionic changes in the culture media, CaP discs and bone slices were pre-incubated for 24 h in complete culture medium at 37°C and 5 % CO_2. After collecting and storing the pre-incubation media (day 0), samples were consequently cultivated for another 8 days in complete culture medium under humidified conditions. A media change was performed every other day, and the supernatants were collected at specific time points (day 2, 4, 6 and 8). All collected media were stored at -20°C until analysis.

Calcium concentration was determined using a colorimetric calcium assay (Sigma-Aldrich, MAK022). After centrifugation (5 min, 1500 rpm) of the collected media, supernatants were diluted 1:5 in ultrapure water and mixed with chromogenic substrate solution and assay buffer as indicated in the manufacturer's instruction. Absorbance was measured at 575 nm on a standard microplate reader and compared to a calcium standard curve.

2.2. Osteoclast cultures

Human osteoclast differentiation was performed on CD14+ cells isolated from the peripheral blood of three healthy donors, provided by the EFS (Etablissement Français du Sang) under ethical approval and after receiving informed consent. Human peripheral blood mononuclear cells were isolated from whole blood by Ficoll®-Paque Premium (GE Healthcare, USA) gradient and sorted with CD14 microbeads on LS MACS column (Miltenyi Biotec, Germany). Cell pools enriched in CD14+ monocytes were aliquoted and stored in liquid nitrogen until use, no longer than 6 months.

Mouse osteoclasts were derived from bone marrow precursors from 8–12-week-old BALB/c mice (Charles River Laboratories, Germany). Mice were euthanized and dissected under sterile conditions to retrieve both femurs and tibiae. Epiphyses were cut off, and the medullary cavities were flushed to collect the marrow. To lyse the erythrocytes, the mouse bone marrow was incubated with red blood cell (RBC) lysis buffer (Abcam, UK) for 5 min at room temperature. Bone-marrow-derived precursor cells were freshly used for differentiation experiments.

Human or mouse osteoclasts precursors were seeded onto the pre-incubated CaP discs, bovine bone slices or tissue culture plastic in complete culture medium supplemented with 25 ng/mL (human CD14+) or 30 ng/mL (mouse precursors) recombinant human M-CSF (rh-M-CSF, Milteny Biotech) at a density of $3.125 \times 10^5/cm^2$ and were cultivated for 8 days at 37°C and 5 % CO_2. On day 2, 100 ng/mL of soluble rh-RANKL (Milteny Biotech) or 30 ng/mL recombinant mouse RANKL (rm-RANKL, R&D Systems, USA) was added to induce osteoclast development. A media change was performed every other day, and cell-conditioned media was collected and stored at -20°C for tartrate-resistant acid phosphatase (TRAP) activity assessment. After 8 days, cells were fixed in 10 % formalin (Sigma-Aldrich) for TRAP staining.

2.3. Osteoclast characterization

To monitor osteoclast differentiation throughout the culture period, we evaluated the extracellular acid phosphatase activity (simplified here as TRAP activity) in cell-conditioned media at every media change (days 2, 4, 6, and 8) as numerous studies have shown its suitability for osteoclast differentiation assays and demonstrated a direct correlation to the osteoclast number [21,31,32]. Briefly, TRAP activity was measured using a fluoresence-based approach (EnzChek® Phosphatase Assay Kit, Invitrogen, Thermo Fisher Scientific). After centrifugation of the collected media, supernatant and substrate solution (200 µM 6,8-difluoro-4-methylumbelliferyl phosphate; DiFMUP) were mixed in a ratio of 1:2 according to the manufacturer's instructions. The dephosphorylation reaction was allowed to take place for 15 minutes at 37°C. Fluorescence was measured on a microplate reader (excitation 358 nm; emission 455 nm) and compared to a standard curve of the dephosphorylated product (6,8-difluoro-7-hydroxy-4-methylcoumarin; DiFMU).

For TRAP staining, we followed a previously described protocol [30]. Briefly, formalin-fixed samples were incubated for 30 minutes at 37°C in a TRAP buffer containing 40 mM sodium acetate and 10 mM sodium tartrate (pH=5). The buffer was removed, and a 1:1 mixture of acetone and 100 % ethanol was applied for 30 seconds for cell permeabilization. The samples were left to air dry for 2 minutes and incubated with the TRAP staining solution for 30 minutes at 37°C. The reaction was stopped with distilled water and samples were imaged using an optical microscope (Olympus IX73 with an Olympus DP74 color camera, Olympus, Japan). All reagents used for TRAP staining were purchased at Sigma-Aldrich.

2.4. hMSC isolation and culture

hMSCs were isolated and characterized by the *Institut für Klinische Transfusionsmedizin und Immungenetik* (IKT) of Ulm (Germany) as previously described [33]. Detailed information on the cells used in the present study can be found as supplementary material of the above-mentioned article (donor ID 7554). Briefly, hMSCs were isolated from the iliac crest of a healthy male donor (age: 22), after receiving informed consent according to the Declaration of Helsinki and ethical approval from the local ethical committee. hMSCs were expanded in culture at 37°C and 5 % CO_2 in basal culture medium consisting of α-MEM supplemented with 100 U/ml penicillin and 100 μg/ml streptomycin, 5 % pooled human platelet lysate (PL), and 1 IU/ml medical grade heparin. PL from several blood donors was prepared by IKT Ulm. For phenotypic characterization of hMSCs, flow cytometry and tri-lineage differentiation capacity were assessed. In the following animal experiment, hMSCs were used at passage 3.

2.5. Ectopic implantation model

Animal experiments followed the European recommendations (2010/63/UE) and were authorized by the local ethical committee (project #6575) *and* the National competent authority *(Ministère de l'Enseignement Supérieur de la Recherche et de l'Innovation*, APAFIS#6575-2016083011049070 v3). Six weeks old NMRI nude female mice were purchased from Janvier Labs (France) and were housed in filter cages with *ad libitum* access to food and water.

For ectopic implantation, mice received a subcutaneous injection of buprenorphine (0.03 mg/kg; Axience, France) as an analgesic 30 min before surgery and were placed under general anesthesia by inhalation of isoflurane (induction: 3.5 %; maintenance: 2.5 % at 1L/min oxygen; Axience). To prevent hypothermia, the animal's temperature was sustained by a heating plate (37°C) during the procedure and recovery. Two vertical incisions were made at the dorsal back of the animal. After that, a subcutaneous pocket was made using blunt scissors, implant materials were placed, and wounds were closed using non-resorbable sutures (Filapeau 4/0, Peters Surgical, France). Additional analgesic injections could be performed in the first 48h after surgery if signs of pain were noticed.

Animals were randomly and equally assigned to the treatment groups (n=5). Each mouse received two implants, the biomaterial alone in the form of granules (50 mg) and the material (50 mg) pre-seeded with 2×10^6 hMSCs in serum-free media. Cells were seeded onto CaP granules in serum-free αMEM and implanted after 1-2 h. After 2, 4, or 8 weeks, animals were sacrificed, subcutis implants were harvested and immediately fixed in 4 % formol solution (Sigma-Aldrich).

2.6. Histology and histomorphometry

Fixed explants were decalcified in PBS containing 4.13 % ethylenediaminetetraacetic acid (EDTA) and 0.2 % paraformaldehyde (pH 7.4) using a microwave automat (KOS Histostation, Milestone Med. Corp., USA). Samples were then dehydrated in ascending grades of ethanol, followed by a butanol bath in an automated dehydration station (STP-120, MM France) and embedded in paraffin (Histowax, Histolab, Sweden). Thin sections (3 µm) in the center of each construct were prepared on a microtome (RM2255, Leica, Germany) and deparaffinized before staining.

For bone formation, deparaffinized histological sections were stained by Masson's Trichrome method (Fuchsin Ponceau F/C0443, Orange G F/C0082, Light Green F/C0702, all from MM France). In this staining, collagen appears green, cell nuclei appear dark blue/black, and cytoplasm, erythrocytes, and muscle red.

To study the impact on osteoclast recruitment and function, we stained the histological sections for TRAP and cathepsin K (CTSK). To visualize TRAP, sections were incubated with a staining solution consisting of 1 mg/mL naphthol AS-TR phosphate, 60 mmol/L N,N-dimethylformamide, 100 mmol/L sodium tartrate, and 1 mg/mL fast red TR salt solution (Sigma-Aldrich) for 1 h, followed by hematoxylin counterstaining for cell nuclei. For CTSK detection, slides were deparaffinized and incubated overnight at 60°C in Tris EDTA pH=9 buffer for antigen retrieval. Endogenous peroxidases were blocked by incubating the slides in 3 % H_2O_2 for 15 min and non-specific sites were saturated by a blocking solution (2 % goat serum, 1 % BSA in TBS pH7.6, 0.05 % Tween) for 30 min. The primary antibody (rabbit polyclonal anti-cathepsin K, Abcam, ab 19027) was diluted in the blocking solution (1:4000) and applied on the slides for 2 hours at room temperature. The secondary antibody (biotinylated goat anti-rabbit, Dako, Germany, E0432, 1:400) was applied for 1 hour at room temperature. Staining was revealed by incubation with streptavidin/horseradish peroxidase conjugate (Dako, P0397), followed by a 3,3' diaminobenzidine solution (DAB Quanto, Thermo Scientific, TA-125-QHDX).

Implanted human cells were tracked using an antibody targeting vimentin, a type II intermediate filament protein following the same procedure as for the CTSK staining. While non-specific to human cells, the antibody was shown not to cross-react with mouse tissues (data not shown) and used successfully in a similar context in a previous study [34]. The incubation with the primary monoclonal mouse anti-vimentin antibody (1:800 dilution, Dako, M0725) was carried out over 1 hour followed by 45 minutes with the secondary goat anti-mouse biotinylated antibody (1:500 dilution, Dako, E0433). Staining was revealed by incubation with streptavidin/horseradish peroxidase conjugate (Dako, P0397) followed by 3,3' diaminobenzidine solution (DAB Quanto, Thermo Scientific, TA-125-QHDX).

All stained slides were scanned using a NanoZoomer (Hamamatsu, Japan) to analyze new bone formation, osteoclastogenesis, and the presence of hMSCs.

2.7. Histomorphometry

Masson's Trichrome stained slides were manually segmented for newly formed bone in the explant using Adobe Photoshop (Adobe, USA). Bone formation was calculated by dividing the bone area (nB.Ar) by the available area (Av.Ar = total explant area - biomaterials surface area) and is presented as a percentage (nB.Ar/Av.Ar %).

TRAP-positive areas (TRAP+ area %) and the number of hMSCs from vimentin immunostaining (Vim+/Tt.Ce %) were calculated after image processing using QuPath [35]. Briefly, for TRAP staining, color segmentation was performed, and stained (red) pixels were counted and compared to the total pixel count to determine a percentage of the TRAP+ area. For vimentin, the total numbers of cells (Tt.Ce) were detected according to their hematoxylin-counterstained nuclei and cell expansion was set from each nucleus to consider the cytoplasm compartment. Finally, a thresholding on vimentin staining was determined and the percentage of vimentin-positive (Vim+) cells was calculated as a ratio of the total cell number (Tt.Ce).

2.8. Statistical analysis

Data presentation and statistical analysis were performed using GraphPad Prism 9.0 (GraphPad Software, USA). *In vitro* results are presented as mean (± SD). Data quantifying *in vivo* osteoclastogenesis, bone formation and hMSC survival are shown in box plots as median with range. Statistical differences were determined using either one-way ANOVA with Tukey's post hoc test for multiple

Table 1
Phase quantification, skeletal density, specific surface area (SSA) and porosity (%) of all studied biomaterials.

Material	HA (%)	β-TCP (%)	Skeletal density (g/mL)	SSA (m^2/g)	Porosity (%)
β-TCP	0.0	100.0	3.08 ± 0.01	0.31 ± 0.01	40.9 ± 0.4
BCP 20/80	19.9	80.4	3.11 ± 0.02	0.59 ± 0.01	51.3 ± 0.5
BCP 60/40	56.0	44.0	3.13 ± 0.01	0.40 ± 0.01	49.3 ± 0.5
HA	97.2	2.8	3.18 ± 0.07	0.53 ± 0.01	50.3 ± 0.5

comparisons in case of multiple groups or two-way ANOVA with Šidák post hoc test for multiple comparisons in case of multiple biomaterials with and without hMSCs. Differences were considered statistically significant when $p < 0.05$.

Further data analyses were conducted to evaluate potential correlations between *in vitro* and *in vivo* osteoclast assessments and across the entire *in vivo* dataset. Therefore, we plotted the mean values of the individual assessments and calculated the Pearson's correlation coefficient (r). Overall correlations across the *in vivo* dataset are presented as a heat map. Relevant correlations including their corresponding Pearson's correlation coefficients (r) and coefficients of determination (R^2) were further shown in separate graphs as mean per material (± SEM). A *p*-value of < 0.05 was considered statistically significant.

3. Results

3.1. Characterization of biomaterials

Fig. 1A shows the XRD patterns of the studied materials, which are quantified in Table 1. While HA and β-TCP showed only the characteristic peaks of each phase, the biphasic nature of the materials was observed for both BCP 60/40 and BCP 20/80. The values of skeletal density obtained by helium pycnometry (Table 1) corresponded to the theoretical densities of these compounds. The specific surface area (SSA, m^2/g) and porosity (%) are depicted in Table 1. It can be observed that β-TCP shows the lowest SSA and porosity. Fig. 1B shows the pore entrance size distributions. For all groups, porosity is in the range of the microporosity (1-10 µm), as additionally observed by SEM imaging (Fig. 1C).

When soaked in culture media, the four CaP compositions presented different profiles of calcium release or uptake over 8 days (Fig. 1D). The control bone slice and BCP composites showed only minor interaction with the calcium in the culture media causing only little changes in the calcium content. HA discs tended to release calcium in the early days, with a significant increase at day 4, resulting in a mean calcium concentration of 4.27 mM before decreasing below the standard level. On the contrary, β-TCP discs demonstrated a strong uptake of calcium during pre-incubation, with an average calcium concentration of 0.72 mM, before returning to the basal level on day 2.

3.2. In vitro *osteoclast differentiation*

In vitro osteoclast formation was studied using human CD14+ of three healthy donors and mouse precursor cells. Cultures of human CD14+ monocytes differentiated in the presence of M-CSF and RANKL into TRAP+ osteoclasts on plastic, bone and all tested CaP materials by day 8 (Fig. 2A). Overall, the cell density appeared lower on HA materials than all others, with fewer and smaller TRAP+ cells. BCP 60/40, BCP 20/80 and β-TCP showed a regular distribution of TRAP-stained cells with higher numbers. While BCP 60/40 presented TRAP+ cells of similar size, larger cells were frequently observed in BCP 20/80 and β-TCP. A DAPI/Phalloidin staining (Supplementary Fig. 1A) confirmed the observed differences in cell density and morphology. Unlike the typical podosome border of osteoclasts cultured on plastic and bone slices, precursors grown on CaP surfaces formed isolated podosome clusters, making it difficult to delimit cytoplasm and conclude on multinucleation. A 3D reconstruction of the surfaces was done using SEM (Supplementary Fig. 1B) but no clear resorption of the CaP materials could be observed with these culture condition, contrasting with the pits visible on bone surface.

As an indirect measurement of osteoclastogenesis, we detected the TRAP enzymatic activity secreted by cells in the media at every media change (Fig. 2B). All three CD14+ donors showed similar trends for plastic, bone, and CaP materials; however, donor variations led to higher variabilities. On plastic and bone, TRAP activity steadily increased over time as monocytes differentiated into osteoclasts. A plateau in TRAP activity was reached on bone on day 6, whereas cells on plastic further differentiated until day 8. Interestingly, we detected TRAP on day 2 before starting RANKL stimulation, which was higher when cultured on CaP materials, albeit not significant. BCP 60/40, BCP 20/80, and β-TCP enabled osteoclastic differentiation to a more considerable extent compared to controls and HA. This was evident from day 4, suggesting a potential pro-osteoclastogenic effect of these materials. Whereas most CaP materials presented a stable activity around day 4 or 6, TRAP activity levels on HA dropped from day 4 and finished lower than at the beginning. Although not significant, the maximum TRAP activity was reached on BCP 60/40, followed by BCP 20/80 and β-TCP. The lowest value was observed on HA. Only differences in TRAP activity between BCP 60/40 and HA were statistically significant.

To test whether the differentiation of mouse osteoclasts was affected differently by CaP materials, we cultured mouse bone-marrow-derived osteoclast precursors and differentiated them using M-CSF and RANKL (Fig. 3). Qualitative image analysis of TRAP-stained cultures revealed similar trends in cell density and morphology as human osteoclasts with widespread and large osteoclasts on plastic and smaller, irregularly shaped osteoclasts on bone and CaPs. The maximum TRAP level was measured for β-TCP, followed by BCP 60/40 and BCP 20/80. Discs composed of HA did not support mouse osteoclast precursor attachment and differentiation, whereby HA differed significantly from all other tested CaP materials. While osteoclast differentiation was similar between β-TCP and bone, TRAP activity was significantly reduced for BCP 20/80 at all time points. The same tendency was observed with BCP 60/40 but with a slightly higher overall TRAP activity. Further, osteoclast activity was confirmed by analyzing CTSK in cell-conditioned media using western blotting (Supplementary Fig. 2). We found comparable CTSK protein levels between bone, both BCP and β-TCP, whereas CTSK was not detectable in HA, corroborating our findings from the TRAP assays.

3.3. In vivo *osteoclastogenesis and bone formation*

After subcutaneous implantation of CaP granules with or without hMSCs in NMRI nude mice, samples were retrieved after 2, 4, and 8 weeks, and were analyzed for osteoclasts and bone formation. Multinucleated cells of monocyte/macrophage origin were typically present at the biomaterial surface. The characterization of their potential osteoclastic phenotype was performed by TRAP and

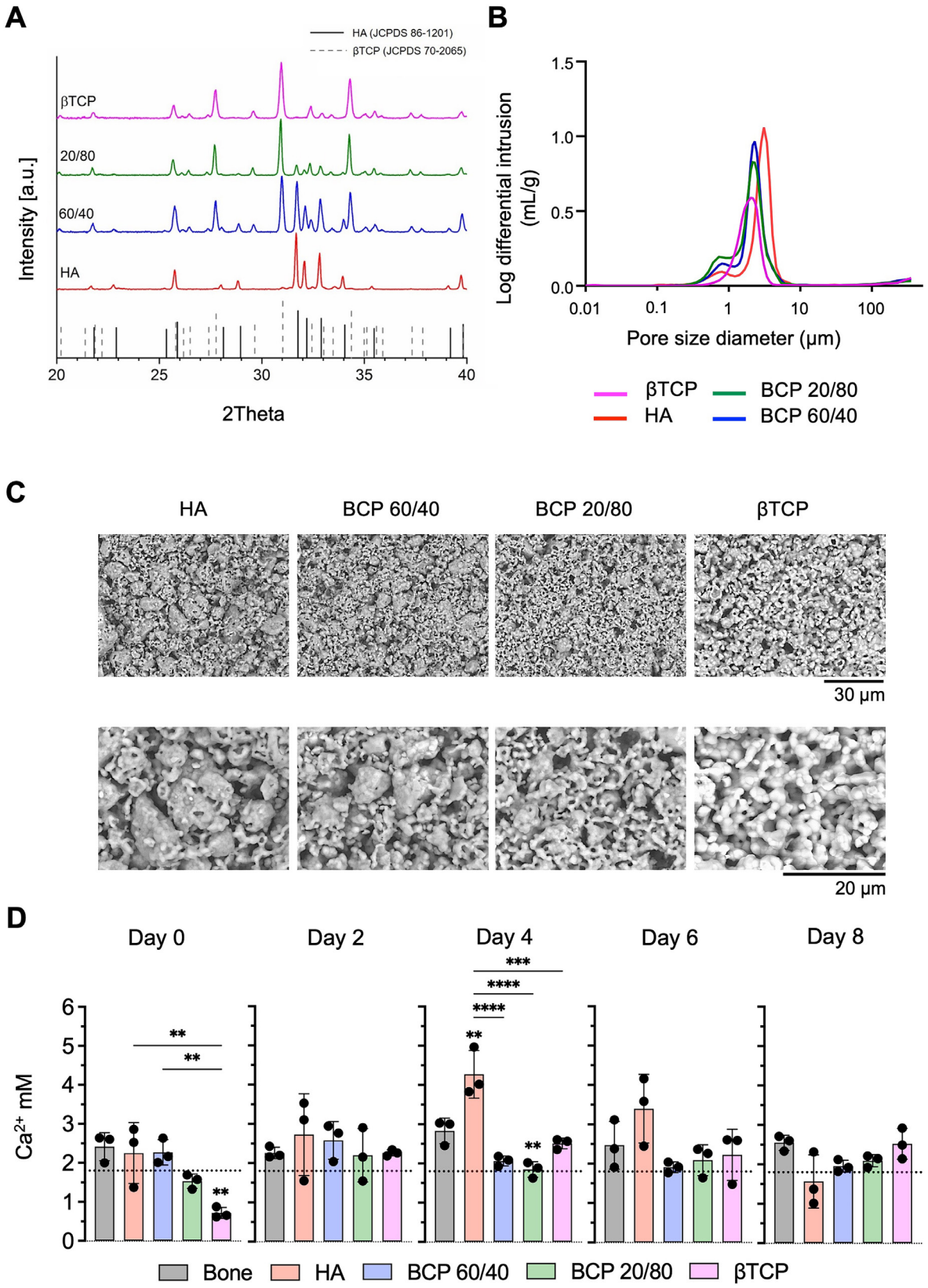

Fig. 1. Characterization of the CaP discs. (A) XRD patterns of all studied materials. (B) Pore entrance size distribution measured by MIP of all studied materials. (C) Representative scanning electron microscopy (SEM) images at two different magnifications demonstrating the surface topography of the tested materials. (D) Quantification of *in vitro* calcium release or adsorption by CaP discs. Supernatants were collected at every media change and analyzed for calcium (Ca^{2+} mM). Time point day 0 reflects the release or adsorption after pre-incubation. Data is presented in absolute values as mean ± SD from one representative experiment ($n = 3$). ** ($p < 0.01$), *** ($p < 0.001$) and **** ($p < 0.0001$) denote statistical differences. Asterisks directly above a bar indicate differences to the bone control. Dashed line represents the basal level of inorganic calcium (Ca^{2+} 1.8 mM) in the complete culture media.

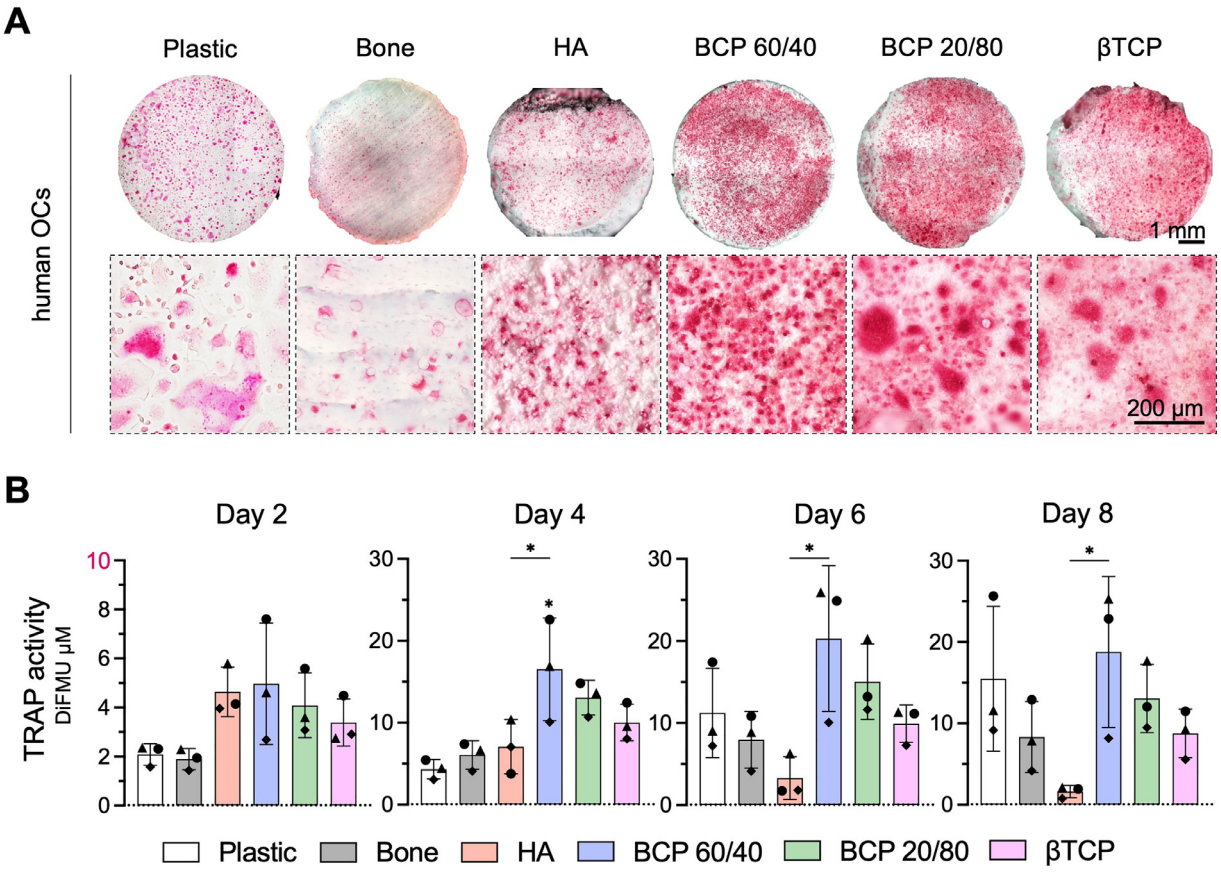

Fig. 2. Differentiation of human CD14+ monocytes to osteoclasts on CaP discs. (A) Representative images of TRAP+ human osteoclasts (OC; stained in red/pink) on plastic, bone, and various CaP discs after 8 days of culture in complete culture media supplemented with 25 ng/mL rh-M-CSF and 100 ng/mL rh-RANKL. (B) Quantification of osteoclast-related TRAP activity in cell culture supernatants as a marker for differentiation measured at every media change (day 2, 4, 6 and 8). TRAP activity (TRAP activity in µM DiFMU) was quantified by enzymatic dephosphorylation and is presented in absolute values as mean ± SD. To indicate donor variability, diverse symbols have been used for identification (donor 1 ●; donor 2 ▲; donor 3 ♦). Each data point represents the mean value of one donor calculated by 3-4 replicates. * ($p < 0.05$) denotes statistical differences. Please note different scale on y-axis!

CTSK staining (Fig. 4A), showing positively stained cells for both markers on all CaPs pre-seeded with hMSCs. In the absence of hMSCs, multinucleated cells were oversized, negative for TRAP, and either unstained or slightly positive for CTSK as observed in Fig. 4A (red arrows). The highest amount of TRAP+ and CTSK+ multinucleated cells was evident after 2 weeks of implantation with a steady reduction until 8 weeks (Supplementary Fig. 3A).

After 2 weeks, the TRAP+ surface area significantly increased for all hMSCs-loaded CaP materials compared to the pristine material, except for HA where the difference was not statistically significant. Moreover, the comparison between the materials showed a significant difference between cell-loaded HA and β-TCP ($p < 0.05$), while BCP 60/40 and BCP 20/80 demonstrated a similar response. Further, no differences were observed in β-TCP vs. BCP 60/40 or 20/80, and HA vs. BCP 60/40 or 20/80. At 4 and 8 weeks, the multinucleated osteoclasts tend to disappear. Interestingly, the TRAP+ surface area on hMSCs-HA granules was nearly maintained from 2 to 4 weeks, whereas it profoundly dropped between 80.7 % and 90.5 % for all other materials (Fig. 4B; Supplementary Table 1).

Conditions that supported early osteoclastogenesis also resulted in prompt ectopic bone formation. New bone detected by Masson's Trichrome staining (Fig. 5A; Supplementary Fig. 3B; bone: stained green) was predominantly attached to the granules' surface, partially bridging to other particles. Newly formed bone was composed of mineralized highly condensed collagen with osteocytes and exhibited some hematopoietic bone marrow areas.

Quantitative evaluation (Fig. 5B; Supplementary Table 2) of bone formation revealed ascending levels of new bone (nB.Ar/Av.Ar %) over time, but only in hMSCs-loaded CaP materials. After 2 weeks, minor bone quantities were detected in cell-containing HA and β-TCP implants. From 2 to 4 weeks, a substantial increase in new bone was observed for hMSCs-loaded β-TCP, which was statistically higher compared with all other materials. Bone quantities were enhanced or maintained until 8 weeks post-implantation. Only differences in the bone area between cell-loaded β-TCP and HA were statistically significant ($p < 0.05$). No differences were observed in β-TCP vs. BCP 60/40 or 20/80, and HA vs. BCP 60/40 or 20/80.

3.4. In vivo *hMSCs survival*

To identify engrafted human MSCs and follow their survival, we used an immunohistochemical approach to stain the vimentin protein, an intermediate filament expressed by mesenchymal cells (Fig. 6, hMSCs: stained brown). CaP materials implanted without hMSCs did not exhibit any staining at all time points (data not shown), ensuring the absence of human MSCs migration from the contralateral side and that the antibody did not react to mouse epitopes.

For all cell-loaded materials, large areas of Vim+ cells could be seen on the surface and around the biomaterials after 2 weeks (Fig. 6A). The size of stained areas progressively decreased over

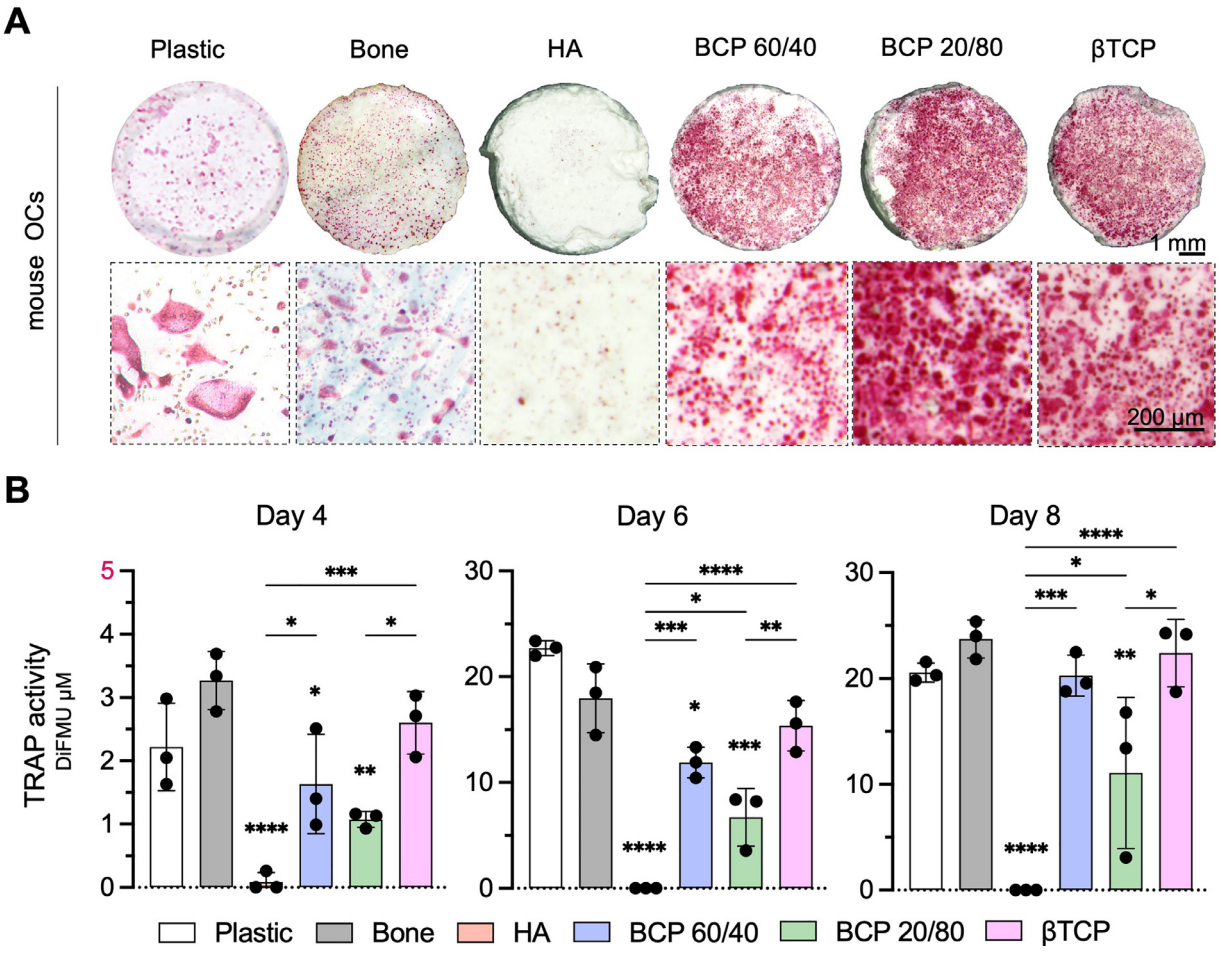

Fig. 3. Differentiation of mouse osteoclast precursors to osteoclasts on CaP discs. (A) Representative images of TRAP+ mouse osteoclasts (OC; stained in red/pink) on plastic, bone and various CaP discs after 8 days of culture in complete culture media supplemented with 30 ng/mL rh-M-CSF and 30 ng/mL rm-RANKL. (B) Quantification of osteoclast-related TRAP activity in cell culture supernatants as a marker for differentiation measured at every media change (day 4, 6 and 8). TRAP activity is presented from day 4, as day 2 did not show any secreted TRAP (data not shown). Activity (TRAP activity in µM DiFMU) was quantified by enzymatic dephosphorylation and is presented in absolute values as mean ± SD (n = 3). Data is graphed from one representative experiment. * ($p < 0.05$), ** ($p < 0.01$), *** ($p < 0.001$) and **** ($p < 0.0001$) denote statistical differences. Asterisks directly above a bar indicate differences to the bone control. Please note different scale on y-axis!

time, down to only a few isolated cells after 8 weeks. When neo-formed bone appeared at 4 and 8 weeks, some human cells could be seen embedded in the mineralized bone matrix but almost none directly on its surface (red arrows). The vast majority of cells located at the surface or embedded in the newly formed bone matrix was therefore of mouse origin (purplish blue cell nuclei). Quantification of the vimentin staining revealed differences in the percentage of human cells at the earliest time point (Fig. 6B; Supplementary Table 3). BCP 20/80 showed a significantly higher amount of hMSCs compared to BCP 60/40 ($p = 0.0242$) and HA ($p = 0.0022$). No difference was observed for β-TCP.

3.5. Data correlation

To evaluate potential correlations between the measured parameters, both *in vitro* and *in vivo*, we calculated the linear correlation using the Pearson's coefficient (r) and the coefficient of determination (R^2) on the mean values per material. First, we compared the TRAP activities from human and mouse *in vitro* osteoclastogenesis assays to *in vivo* osteoclast formation (TRAP area %) 2 weeks after implanting hMSC-engrafted CaP materials, as we observed the strongest staining for TRAP+ osteoclasts and greatest difference between the materials at this time point (Fig. 7A). Interestingly, the positive correlation and linear regression fit was better when *in vitro* mouse osteoclast differentiation was compared to *in vivo* osteoclastogenesis ($r = 0.911$, $R^2 = 0.830$), rather than with human osteoclast differentiation ($r = 0.383$, $R^2 = 0.147$). Although this correlation was not statistically significant ($p = 0.089$), our results indicate that mouse osteoclast cultures could predict the *in vivo* osteoclastic response to MSC-CaP-mediated bone formation in an ectopic mouse model better than *in vitro* human osteoclast assays.

Focusing on *in vivo* parameters, we created a correlation matrix across the entire *in vivo* dataset by determining the relationship between all tested time points and variables (Supplementary Fig. 4). To test whether early osteoclastic response influences bone formation, we observed the relationship between osteoclastogenesis at 2 weeks (TRAP+ area %) and the main outcome, bone formation (nB.Ar/Av.Ar %), at 8 weeks after implanting CaP materials with hMSCs. It showed a strong positive and significant correlation ($r = 0.952$, $p = 0.048$, $R^2 = 0.906$) (Fig. 7B).

The contribution of hMSCs to bone formation was evaluated by associating the relative numbers of hMSCs (Vim+/Tt.Ce %) at all time points to bone formation at 8 weeks (Fig. 7B). We found that the early hMSC presence moderately related to bone formation (2 weeks vs. 8 weeks; $r = 0.575$, $p = 0.425$, $R^2 = 0.331$). However, when exploring the other combinations, hMSCs even negatively correlated with late bone formation (Supplementary Fig. 5).

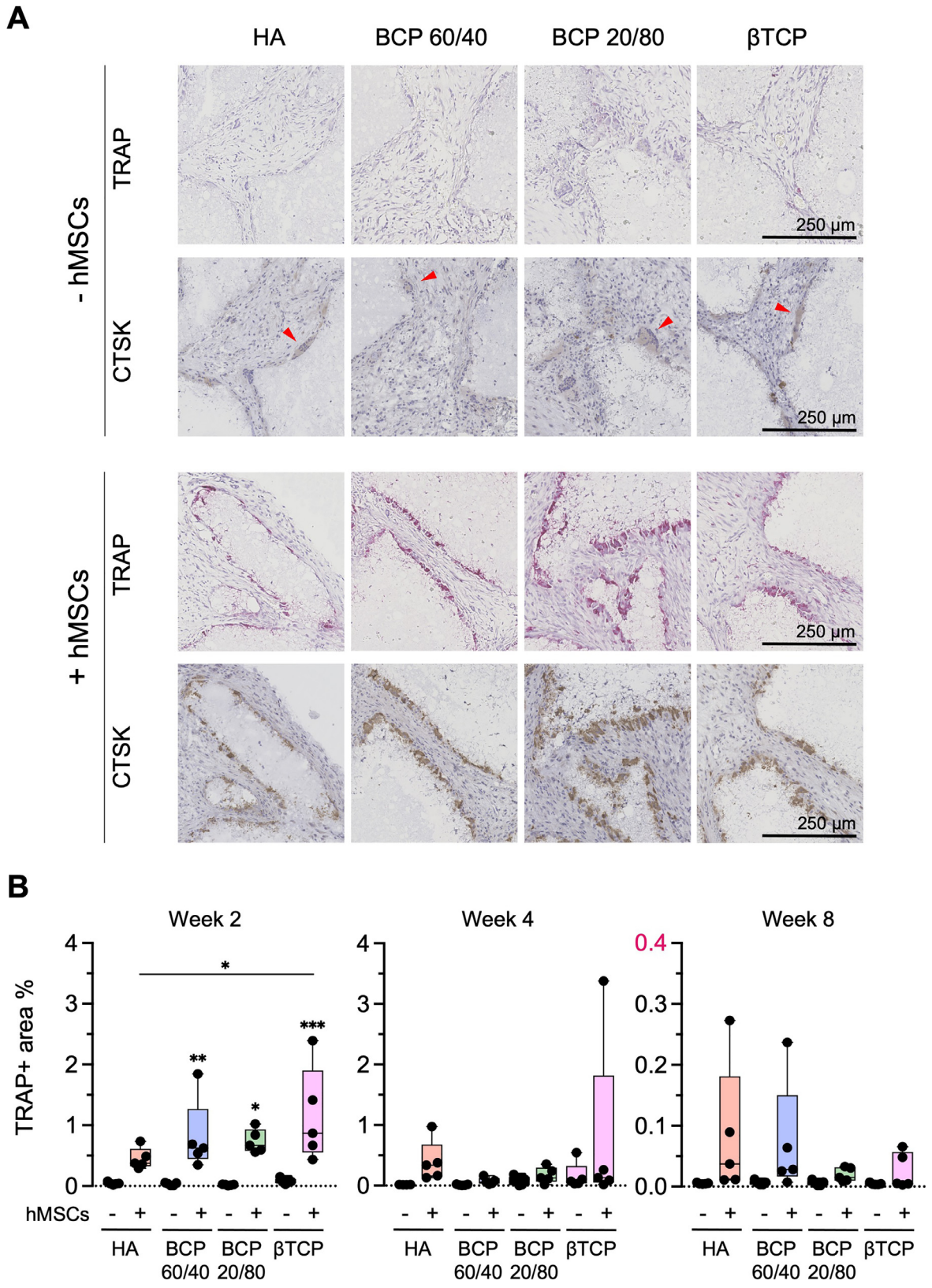

Fig. 4. Effect of CaP materials and hMSCs on osteoclast formation *in vivo*. CaP granules alone or in combination with hMSCs were subcutaneously implanted in nude mice and analyzed after 2, 4 and 8 weeks. (A) Representative images of TRAP- and CTSK-stained cross-sections explanted after 2 weeks. TRAP+ stained cells appear pink, while CTSK+ cells are visible in brown. Red arrow heads indicate oversized, TRAP negative, and unstained or slightly CTSK+ stained multinucleated cells in CaP materials alone. - hMSCs: CaP granules without hMSCs; + hMSCs: CaP granules with hMSCs. (B) Histomorphometric analysis of osteoclastogenesis. Osteoclast formation was calculated as TRAP+ area (%) by dividing the TRAP+-stained area by the total explant area. CaP granules alone are designated as – and with hMSCs as +. Data is shown as median and range ($n = 5$), and * ($p < 0.05$), ** ($p < 0.01$), *** ($p < 0.001$) denote statistical differences. Asterisks directly above the bar indicate differences between ± hMSCs within a CaP group. Please note different scale on y-axis!

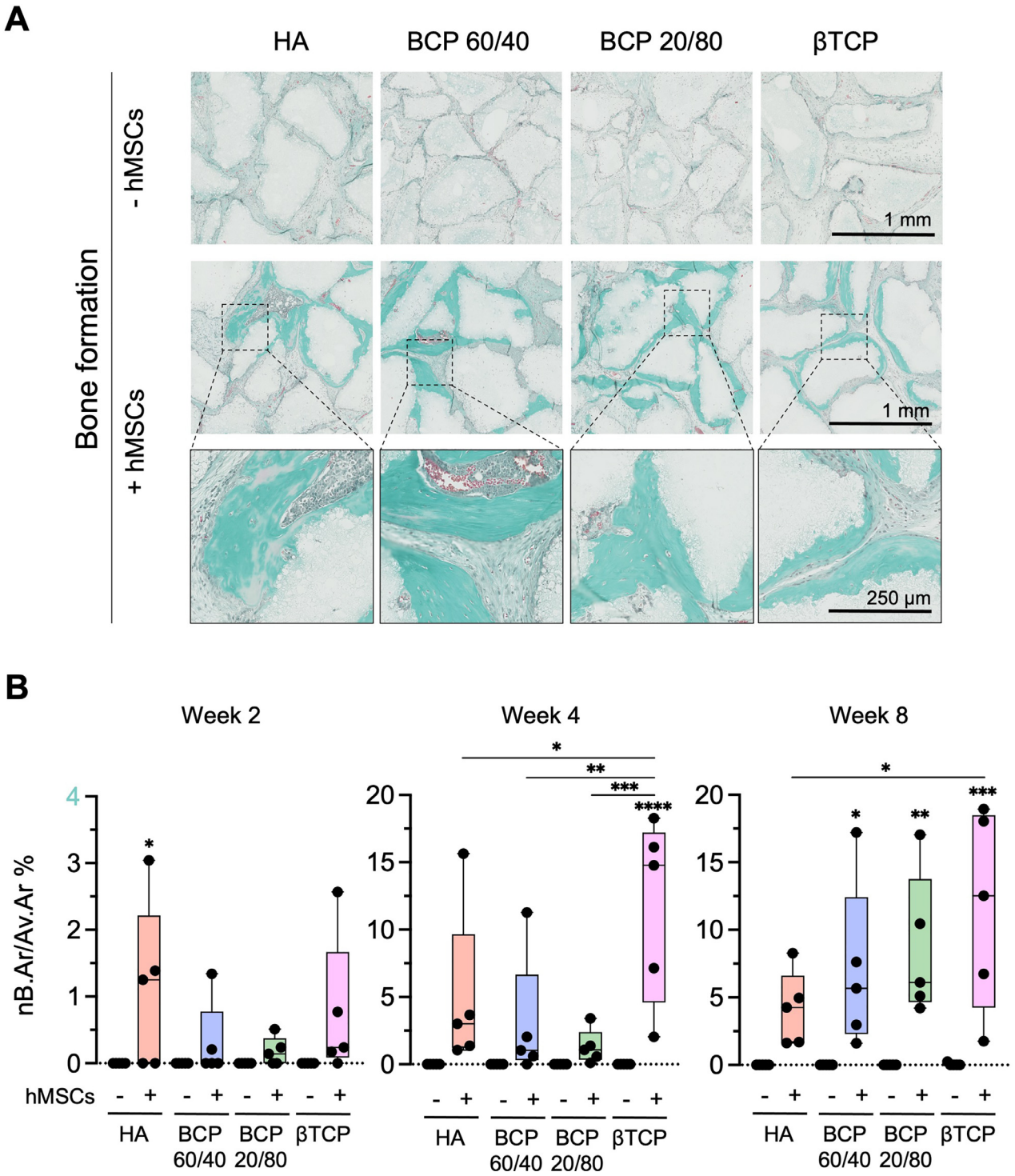

Fig. 5. Evaluation of bone formation by CaP materials and hMSCs *in vivo*. CaP granules alone or in combination with hMSCs were subcutaneously implanted in nude mice and analyzed after 2, 4 and 8 weeks. (A) Representative images of Masson's Trichrome stained cross-sections explanted after 8 weeks. In this staining, newly formed bone (= mineralized highly condensed collagen with osteocytes) appears green. - hMSCs: CaP granules without hMSCs; + hMSCs: CaP granules with hMSCs. (B) Histomorphometric analysis of new bone formation. New bone formation was calculated by dividing the bone area by the available area (= total explant area - biomaterials surface area) (nB.Ar/Av.Ar %). CaP granules alone are designated as – and with hMSCs as +. Data is presented as median and range ($n = 5$), and * ($p < 0.05$), ** ($p < 0.01$), *** ($p < 0.001$) and **** ($p < 0.0001$) denote statistical differences. Asterisks directly above a bar indicate differences between ± hMSCs within a CaP group. Please note different scale on y-axis! nB.Ar: new bone area; Av.Ar: available area.

Finally, to determine if there was a link between osteoclast formation and hMSCs in the early phase after implantation, relative values of osteoclastogenesis and hMSCs were correlated at 2 weeks after implanting hMSC-loaded CaPs revealing a weak positive relation ($r = 0.341$, $p = 0.660$, $R^2 = 0.116$).

4. Discussion

The overall goal of the present study was to evaluate whether compositional variations in CaP materials can affect the osteoclastic response and thereby modulate bone formation in combination

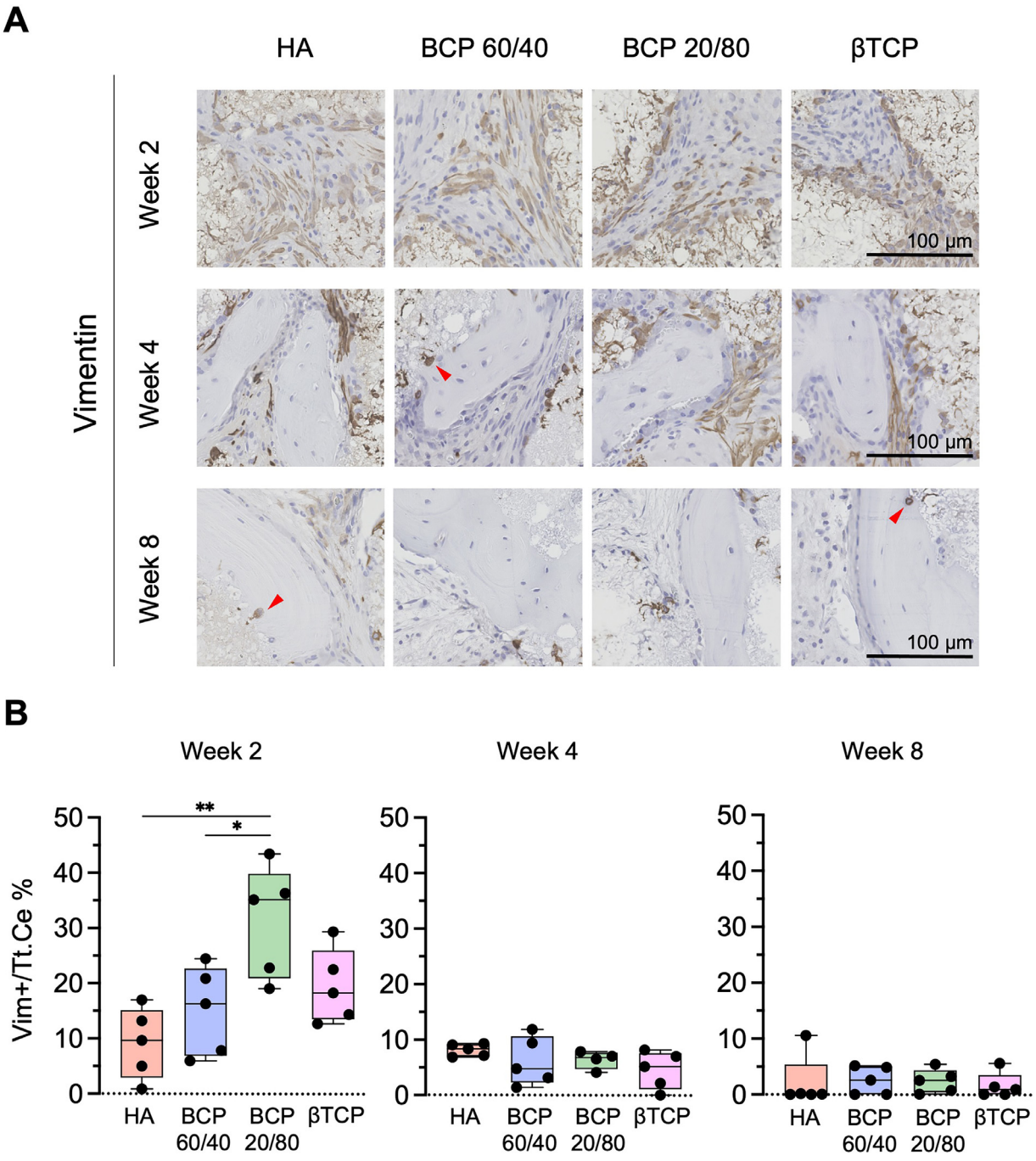

Fig. 6. Representation and quantification of hMSCs engrafted in CaP materials. CaP granules were pre-seeded with hMSCs, subcutaneously implanted in nude mice and analyzed after 2, 4 and 8 weeks. (A) Representative images after immunohistochemical staining for human vimentin. Vimentin+ stained human cells appear brown, whereas cell nuclei from mouse cells are stained purplish blue. Red arrow heads indicate human cells embedded in newly formed bone. (B) Quantification of vimentin+ hMSCs in histological cross-sections. Data is shown as percentage of vimentin+ cells per total cell count (Vim+/Tt.Ce %) and presented as median and range (n = 4-5). * ($p < 0.05$) and ** ($p < 0.01$) denote statistical differences.

with hMSCs. We compared four CaP materials with different HA/β-TCP ratios for their capability to support osteoclasts and bone formation using *in vitro* and *in vivo* models. It is worth highlighting that the preparation of the biomaterials was designed in such a way that their porosity and microstructure were comparable, since the starting powder, the sintering temperature and time were the same for all the compositions. This allows these two variables to be ruled out when analyzing the effect of the material and to focus on the composition. Table 2 summarizes the individual results obtained by the different experimental evaluations using a semiquantitative scoring system. Our main findings herein were (a) a relatively good correlation between *in vitro* mouse osteoclast differentiation and *in vivo* osteoclastogenesis (Fig. 7A), (b) increased osteoclast (Fig. 4) and bone formation (Fig. 5) in hMSC-loaded CaP material (β-TCP > biphasic CaPs > HA), (c) a strong positive correlation between the number of early osteoclasts and lately formed bone (Fig. 7B), and (d) a weaker correlation between hMSCs survival and bone formation in the subcutaneous mouse model (Fig. 7B, Supplementary Fig. 5).

Multiple studies emphasize the pivotal role of osteoclasts in osteoinduction and particularly in the context of hMSCs and CaP materials reinforcing the need of including osteoclast-biomaterial in-

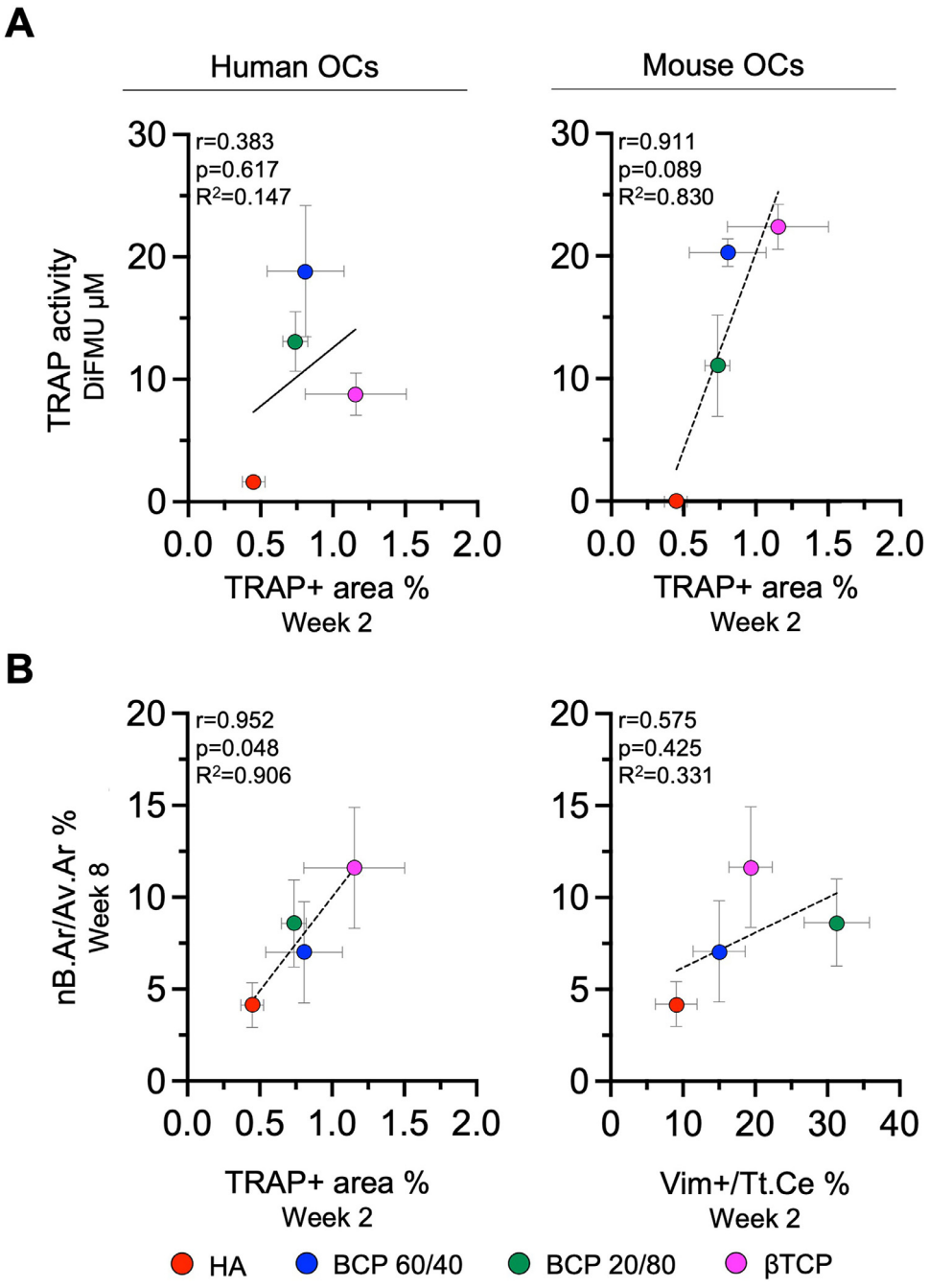

Fig. 7. Correlation analysis. (A) *In vitro* human and mouse osteoclast (OC) differentiation assays and *in vivo* osteoclastogenesis. The correlation was analyzed by plotting the mean (± SEM) of *in vitro* TRAP activities at the study endpoint (day 8) against *in vivo* osteoclast levels 2 weeks after implanting CaP materials and hMSCs.(B) Correlation of *in vivo* assessments after implantation of hMSC-engrafted CaP materials showing bone formation (nB.Ar/Av.Ar %; 8 weeks) vs. early osteoclastogenesis (TRAP+ area %; 2 weeks) or relative numbers of hMSCs (Vim+/Tt.Ce %; 2 weeks). Data is presented as mean ± SEM, and Pearson's coefficients (r), p values and coefficients of determination (R^2) are displayed in each graph.

teractions in biological compatibility profiling of biomaterials for bone repair [9,19,36]. Herein, we used mononuclear precursors from two different sources, mouse bone marrow and human peripheral blood monocytes, and differentiated them towards osteoclasts on the biomaterials' surface in a differentiation medium containing M-CSF and RANKL. Osteoclasts developed on all CaPs to varying degrees depending on material composition and origin. In this work, we used the extracellular TRAP activity as a quantitative parameter of the osteoclast differentiation profile from the mononuclear precursors because the irregular-shaped surfaces (as shown in Fig. 1B) of the CaPs made it highly difficult, if not impossible, to perform an absolute counting of TRAP+ multinucleated cells under a light microscope at the study endpoint. Cells from both species showed a similar affinity for β-TCP-containing materials over pure HA, which clearly hindered differentiation. While human osteoclasts favored BCP 60/40, mouse-derived osteoclasts preferred pure β-TCP. Although human and mouse cultures differed in the response to CaPs, one thing was common to them both: osteoclast development on β-TCP was comparable to the physiological substrate, bone. The overall preference of osteoclasts for β-TCP-containing materials is in agreement with studies conducted by Shiwaku et al [27,37]. Both *in vitro* studies demonstrated that in-

Table 2
Summary of the individual results obtained by our *in vitro* and *in vivo* models. A scoring system was used to compare the individual assays (- = no effect; + = mild effect; ++ = medium effect; +++ = strong effect). Data from *in vitro* human and mouse osteoclast differentiation testing were combined for a common finding. For individual results refer to Figs. 2 and 3 (*in vitro* osteoclast differentiation), Fig. 6 (hMSC survival), Fig. 4 (*in vivo* osteoclastogenesis) and Fig. 5 (bone formation); * = scoring was based on the data set recorded 2 weeks after implantation; # = scoring was based on the data set recorded 8 weeks after implantation; OC: osteoclast

	In vitro	*In vivo*		
Material	OC differentiation	hMSC survival*	Osteoclastogenesis*	Bone formation#
HA	-	+	+	+
BCP 60/40	++	++	++	+
BCP 20/80	++	+++	++	++
β-TCP	++	++	+++	+++

creasing the concentration of HA negatively affected the osteoclastogenic potential of mouse bone marrow-derived precursors and reduced the number of osteoclasts and expression of osteoclastic coupling factors that promote osteoblast differentiation and function.

When biomaterials were subcutaneously implanted with hMSCs in immunocompromised mice, all CaPs facilitated osteoclastogenesis, but material composition significantly affected the outcome. Specifically, β-TCP promoted osteoclastogenesis, and although HA supported it, it was to a much lesser extent. Consistently, HA also prevented osteoclast differentiation *in vitro*. This is in line with our previous study comparing biomimetic calcium deficient HA and sintered β-TCP scaffolds engrafted with hMSCs [34]. We hypothesize that the suboptimal *in vitro* performance of HA can be explained by the physico-chemical phenomenon that the surface of CaPs endures a dissolution-precipitation cascade where ions are transferred from the solid phase of the material into the aqueous phase, i.e., cell culture medium or body fluid, and vice versa [38]. Although this exchange encompasses both calcium and phosphate, in this work we focused on Ca^{2+} as an indicator of the reactivity of the material. We attributed the adverse effect of HA to the high Ca^{2+} release at day 4, which was in line with the decline in osteoclast number and TRAP activity, and an acidic pH shift in the culture medium observed by its color change (from red-pink to yellow); thereby, HA created an unfavorable environment for cell survival and osteoclast differentiation in our culture system. For future *in vitro* studies involving pure HA materials, it could be helpful to increase either the media volume in the culture dish or the renewing frequency. Nevertheless, the differentiation efficiency of mouse osteoclasts on the four materials *in vitro* matched well the formation of osteoclasts *in vivo* after 2 weeks of implantation (Fig. 7A). This strong predictive value encourages future research to have *in vitro* osteoclast differentiation assays incorporated in the early evaluation steps of novel CaPs formulations. The correlation of the *in vivo* mouse outcome with human osteoclast culture was logically weaker. It highlights that small differences between species always exist and should be remembered when choosing an animal model or moving toward clinical applications.

In vivo osteoclast formation was only observed when hMSCs were loaded onto the granule biomaterials before transplantation. Subcutis implantation sites treated with the biomaterial alone tend to induce multinucleated giant cells (MNGCs), the hallmarks of the foreign-body reaction, leading to fibrosis and encapsulation of the implant [39]. Ectopically located osteoclasts displayed typical markers as positive TRAP and CSTK activity, while MNGCs were either double negative for both or TRAP-negative and slightly positive for CTSK. Comparable results on osteoclast and MNGC phenotypes have been reported by Ahmed et al., when they implanted β-TCP granules with and without rat bone marrow mesenchymal stem cells (BMSCs) into rat subcutaneous tissue. They associated the presence of osteoclasts and TRAP to the implantation of BMSCs and subsequent osteogenesis, while MNGCs were found in cell-free conditions with a similar phenotype as present herein [40]. In the current study, we observed that CaP materials associated with hMSCs exhibiting pro-osteoclastogenic properties in the early phase after implantation led to enhanced bone formation (β-TCP > biphasic CaPs > HA), albeit only differences between β-TCP and HA were statistically significant. Thus, it reinforces the contention that osteoclasts are the pivotal cells initiating bone healing.

Nevertheless, implanted hMSCs are still required to provide a favorable environment for osteoclastogenesis, and should be introduced in sufficient numbers to lead to bone formation in this model [8,41], although we observed only a weak positive correlation between osteoclastogenesis and hMSC survival at 2 weeks post implantation (Supplementary Fig. 5B). Overall, the numbers of hMSCs drastically decreased at the implantation site over time. However, some were still observed on all materials after 8 weeks. More significant differences between materials were evident at 2 weeks, with the highest percentage of hMSCs on BCP 20/80 (30 %) and the lowest one on pure HA (10 %) which moderately correlated to bone formation. It has been suggested that cell survival promotes a successful outcome [11,42]. Prolonged cell survival in the harsh inflammatory environment after implantation would mean a prolonged release of immune modulators and pro-resolving molecules. However, BCP 20/80 did not induce the highest amount of new bone in our condition and hMSC survival at 4 and 8 weeks even negatively correlated with bone formation (Supplementary Fig. 5A). *In vitro*, we have previously shown that the secretome of hMSCs seeded on CaP materials and apoptotic hMSCs favored RANKL-dependent differentiation of osteoclasts while inhibiting IL-4-induced formation of MNGCs from CD14+ human monocytes [43]. Our data suggests that this effect might be linked to the high secretion of IL-8 and other CXCL chemokines, but the mediators involved *in vivo* remain to be identified. More generally, apoptosis of MSCs could be beneficial for immune modulation [44], partly explaining why their survival does not seem to be the major determinant for bone formation.

We have previously proposed a potential sequence of events in MSC-CaP-mediated bone formation [36] which could be reaffirmed by this study whereby transplanted hMSCs seem to favor the formation of osteoclast rather than inflammatory MNGCs. These formed osteoclasts can then locally trigger a bone remodeling cycle by recruitment of osteoblast precursors from the host. The present work is complementary to other recent studies that have explored the mechanisms underlying the transplantation of CaP materials but with a strong focus on macrophages. For example, Nie et al. investigated the response of macrophages to an osteoinductive TCP and a non-osteoinductive one. They observed a higher macrophage polarization towards M2 and a higher osteoclastogenesis on the osteoinductive material, both *in vitro* and *in*

vivo [45]. Similarly, Li et al. associated M2 polarization and osteoclastogenesis to an efficient ectopic bone formation and they identified the hypoxia-inducible factor 1α as a key mediator in the process [46]. Wang et al. used CaP cements to explore the influence of different calcium to phosphate ratio on osteoinduction. They showed that high phosphate concentration could impair osseointegration by inhibiting RANK-L/RANK binding, thus osteoclastogenesis [47]. Finally, Rana et al. recently showed that the presence of hMSCs in BCP implants changed the composition of the innate immune cell population, both locally and in circulation [48].

5. Conclusion

The novelty presented herein is the direct positive relationship between osteoclastogenesis on CaP materials and bone formation in an *in vivo* model. β-TCP containing materials show higher osteoclast levels both *in vitro* and *in vivo*, and led to greater ectopic bone formation than monophasic HA or BCPs. While hMSCs were indispensable for ectopic bone formation in our subcutaneous model, their survival (at 2 weeks) did not correlate with bone formation (at 8 weeks) and tended to even negatively correlate at later time points. Therefore, designing biomaterials based on their compatibility with osteoclastogenesis seems more relevant than focusing on their relationship with implanted hMSCs. Nevertheless, the communication between implanted hMSCs and immune cells involved in the response to the biomaterials, as well as the following step of osteoclast-mediated recruitment of bone-forming cells remains to be fully understood. A better understanding of the cell-cell interactions as well as the cell-material interactions is essential to design new therapeutic strategies overcoming the technical limitations of cell therapy.

Data availability

Data can be made available by request to the authors.

Fundings

This work was financially supported by the European Commission through the H2020 project ORTHOUNION (Grant Agreement: 733288) and by Campus France and the Austrian's Agency for Education and Internationalisation through the PHC Amadeus 2018 program and the scientific and technological cooperation program "Amadée". PH received a PhD fellowship from the Regional Council Pays de la Loire and the ORTHOUNION project. MAB received fundings from the European Union's Horizon 2020 research and innovation program under the Marie Skłodowska-Curie Individual Fellowship, Grant Agreement No 708711. MPG and CC acknowledge PID2019-103892RB-I00/AEI/10.13039/501100011033 project from the Spanish Ministry of Science and Innovation and the SGR2017-1165 and the ICREA Academia Awards for Excellence in Research from the Generalitat de Catalunya.

Declaration of competing interest

The authors declare that they have no known competing financial interests or personal relationships that could have appeared to influence the work reported in this paper.

CRediT authorship contribution statement

Paul Humbert: Conceptualization, Investigation, Data curation, Formal analysis, Writing – original draft, Writing – review & editing. **Carina Kampleitner:** Conceptualization, Investigation, Data curation, Formal analysis, Writing – original draft, Writing – review & editing. **Julien De Lima:** Investigation, Data curation, Formal analysis, Writing – review & editing. **Meadhbh Á Brennan:** Writing – review & editing. **Irene Lodoso-Torrecilla:** Investigation, Data curation, Formal analysis, Resources, Writing – review & editing. **Joanna Maria Sadowska:** Investigation, Data curation, Formal analysis, Resources, Writing – review & editing. **Frédéric Blanchard:** Supervision, Writing – review & editing. **Cristina Canal:** Formal analysis, Resources, Supervision, Writing – review & editing. **Maria-Pau Ginebra:** Formal analysis, Resources, Supervision, Writing – review & editing. **Oskar Hoffmann:** Conceptualization, Supervision, Writing – review & editing, Funding acquisition. **Pierre Layrolle:** Conceptualization, Supervision, Writing – review & editing, Funding acquisition.

Acknowledgements

The authors are grateful to Céline Charrier, Régis Brion and Barbara Berger for their technical support.

Supplementary materials

Supplementary material associated with this article can be found, in the online version, at doi:10.1016/j.actbio.2024.01.022.

References

[1] K.A. Egol, A. Nauth, M. Lee, H.C. Pape, J.T. Watson, J. Borrelli Jr, Bone grafting: sourcing, timing, strategies, and alternatives, J. Orthop. Trauma 29 (Suppl 12) (2015) S10–S14.
[2] L. Vidal, C. Kampleitner, M.A. Brennan, A. Hoornaert, P. Layrolle, Reconstruction of large skeletal defects: current clinical therapeutic strategies and future directions using 3d printing, Front. Bioeng. Biotechnol. 8 (2020) 61.
[3] A. Ho-Shui-Ling, J. Bolander, L.E. Rustom, A.W. Johnson, F.P. Luyten, C. Picart, Bone regeneration strategies: engineered scaffolds, bioactive molecules and stem cells current stage and future perspectives, Biomaterials 180 (2018) 143–162.
[4] J. Stanovici, L.R. Le Nail, M.A. Brennan, L. Vidal, V. Trichet, P. Rosset, P. Layrolle, Bone regeneration strategies with bone marrow stromal cells in orthopaedic surgery, Curr. Res. Transl. Med. 64 (2) (2016) 83–90.
[5] E. Gomez-Barrena, P. Rosset, F. Gebhard, P. Hernigou, N. Baldini, H. Rouard, L. Sensebe, R.M. Gonzalo-Daganzo, R. Giordano, N. Padilla-Eguiluz, E. Garcia-Rey, J. Cordero-Ampuero, J.C. Rubio-Suarez, J. Stanovici, C. Ehrnthaller, M. Huber-Lang, C.H. Flouzat-Lachaniette, N. Chevallier, D.M. Donati, G. Ciapetti, S. Fleury, M.N. Fernandez, J.R. Cabrera, C. Avendano-Sola, T. Montemurro, C. Panaitescu, E. Veronesi, M.T. Rojewski, R. Lotfi, M. Dominici, H. Schrezenmeier, P. Layrolle, Feasibility and safety of treating non-unions in tibia, femur and humerus with autologous, expanded, bone marrow-derived mesenchymal stromal cells associated with biphasic calcium phosphate biomaterials in a multicentric, non-comparative trial, Biomaterials 196 (2019) 100–108.
[6] C. Gjerde, K. Mustafa, S. Hellem, M. Rojewski, H. Gjengedal, M.A. Yassin, X. Feng, S. Skaale, T. Berge, A. Rosen, X.Q. Shi, A.B. Ahmed, B.T. Gjertsen, H. Schrezenmeier, P. Layrolle, Cell therapy induced regeneration of severely atrophied mandibular bone in a clinical trial, Stem Cell Res. Ther. 9 (1) (2018) 213.
[7] E. Gomez-Barrena, N. Padilla-Eguiluz, P. Rosset, F. Gebhard, P. Hernigou, N. Baldini, H. Rouard, L. Sensebe, R.M. Gonzalo-Daganzo, R. Giordano, E. Garcia-Rey, J. Cordero-Ampuero, J.C. Rubio-Suarez, M.D. Garcia-Simon, J. Stanovici, C. Ehrnthaller, M. Huber-Lang, C.H. Flouzat-Lachaniette, N. Chevallier, D.M. Donati, B. Spazzoli, G. Ciapetti, S. Fleury, M.N. Fernandez, J.R. Cabrera, C. Avendano-Sola, T. Montemurro, C. Panaitescu, E. Veronesi, M.T. Rojewski, R. Lotfi, M. Dominici, H. Schrezenmeier, P. Layrolle, Early efficacy evaluation of mesenchymal stromal cells (MSC) combined to biomaterials to treat long bone non-unions, Injury 51 (Suppl 1) (2020) S63–S73.
[8] M.A. Brennan, A. Renaud, J. Amiaud, M.T. Rojewski, H. Schrezenmeier, D. Heymann, V. Trichet, P. Layrolle, Pre-clinical studies of bone regeneration with human bone marrow stromal cells and biphasic calcium phosphate, Stem Cell Res. Ther. 5 (5) (2014) 114.
[9] A.L. Gamblin, M.A. Brennan, A. Renaud, H. Yagita, F. Lezot, D. Heymann, V. Trichet, P. Layrolle, Bone tissue formation with human mesenchymal stem cells and biphasic calcium phosphate ceramics: the local implication of osteoclasts and macrophages, Biomaterials 35 (36) (2014) 9660–9667.
[10] M. Manassero, J. Paquet, M. Deschepper, V. Viateau, J. Retortillo, M. Bensidhoum, D. Logeart-Avramoglou, H. Petite, Comparison of survival and osteogenic ability of human mesenchymal stem cells in orthotopic and ectopic sites in mice, Tissue Eng. Part a 22 (5-6) (2016) 534–544.
[11] G.E. Salazar-Noratto, G. Luo, C. Denoeud, M. Padrona, A. Moya, M. Bensidhoum, R. Bizios, E. Potier, D. Logeart-Avramoglou, H. Petite, Understanding and leveraging cell metabolism to enhance mesenchymal stem cell transplantation survival in tissue engineering and regenerative medicine applications, Stem Cells 38 (1) (2020) 22–33.

[12] R. Dimitriou, E. Tsiridis, P.V. Giannoudis, Current concepts of molecular aspects of bone healing, Injury 36 (12) (2005) 1392–1404.
[13] H. Schell, J. Lienau, D.R. Epari, P. Seebeck, C. Exner, S. Muchow, H. Bragulla, N.P. Haas, G.N. Duda, Osteoclastic activity begins early and increases over the course of bone healing, Bone 38 (4) (2006) 547–554.
[14] N.A. Sims, T.J. Martin, Osteoclasts provide coupling signals to osteoblast lineage cells through multiple mechanisms, Annu. Rev. Physiol. 82 (2020) 507–529.
[15] A. Barba, A. Diez-Escudero, M. Espanol, M. Bonany, J.M. Sadowska, J. Guillem–Marti, C. Ohman-Magi, C. Persson, M.C. Manzanares, J. Franch, M.P. Ginebra, Impact of biomimicry in the design of osteoinductive bone substitutes: nanoscale matters, ACS. Appl. Mater. Interfaces. 11 (9) (2019) 8818–8830.
[16] Y. Raymond, C. Lehmann, E. Thorel, R. Benitez, A. Riveiro, J. Pou, M.C. Manzanares, J. Franch, C. Canal, M.P. Ginebra, 3D printing with star-shaped strands: A new approach to enhance in vivo bone regeneration, Biomater. Adv. 137 (2022) 212807.
[17] M.P. Ginebra, M. Espanol, Y. Maazouz, V. Bergez, D. Pastorino, Bioceramics and bone healing, EFORT. Open. Rev. 3 (5) (2018) 173–183.
[18] N. Kondo, A. Ogose, K. Tokunaga, H. Umezu, K. Arai, N. Kudo, M. Hoshino, H. Inoue, H. Irie, K. Kuroda, H. Mera, N. Endo, Osteoinduction with highly purified beta-tricalcium phosphate in dog dorsal muscles and the proliferation of osteoclasts before heterotopic bone formation, Biomaterials 27 (25) (2006) 4419–4427.
[19] N.L. Davison, A.L. Gamblin, P. Layrolle, H. Yuan, J.D. de Bruijn, F. Barrere-de Groot, Liposomal clodronate inhibition of osteoclastogenesis and osteoinduction by submicrostructured beta-tricalcium phosphate, Biomaterials 35 (19) (2014) 5088–5097.
[20] T.L. Arinzeh, T. Tran, J. McAlary, G. Daculsi, A comparative study of biphasic calcium phosphate ceramics for human mesenchymal stem-cell-induced bone formation, Biomaterials 26 (17) (2005) 3631–3638.
[21] N.L. Davison, J. Su, H. Yuan, J.J. van den Beucken, J.D. de Bruijn, F. Barrere-de Groot, Influence of surface microstructure and chemistry on osteoinduction and osteoclastogenesis by biphasic calcium phosphate discs, Eur. Cell Mater. 29 (2015) 314–329.
[22] N.L. Davison, B. ten Harkel, T. Schoenmaker, X. Luo, H. Yuan, V. Everts, F. Barrere-de Groot, J.D. de Bruijn, Osteoclast resorption of beta-tricalcium phosphate controlled by surface architecture, Biomaterials 35 (26) (2014) 7441–7451.
[23] R. Detsch, A.R. Boccaccini, The role of osteoclasts in bone tissue engineering, J. Tissue Eng. Regen. Med. 9 (10) (2015) 1133–1149.
[24] G. Ciapetti, G. Di Pompo, S. Avnet, D. Martini, A. Diez-Escudero, E.B. Montufar, M.P. Ginebra, N. Baldini, Osteoclast differentiation from human blood precursors on biomimetic calcium-phosphate substrates, Acta Biomater. 50 (2017) 102–113.
[25] A. Diez-Escudero, M. Espanol, E.B. Montufar, G. Di Pompo, G. Ciapetti, N. Baldini, M.P. Ginebra, Focus ion beam/scanning electron microscopy characterization of osteoclastic resorption of calcium phosphate substrates, Tissue Eng. Part C. Methods 23 (2) (2017) 118–124.
[26] A. Diez-Escudero, M. Espanol, S. Beats, M.P. Ginebra, In vitro degradation of calcium phosphates: Effect of multiscale porosity, textural properties and composition, Acta Biomater. 60 (2017) 81–92.
[27] Y. Shiwaku, L. Neff, K. Nagano, K. Takeyama, J. de Bruijn, M. Dard, F. Gori, R. Baron, The crosstalk between osteoclasts and osteoblasts is dependent upon the composition and structure of biphasic calcium phosphates, PLoS. One 10 (7) (2015) e0132903.
[28] M.P. Ginebra, E. Fernandez, E.A. De Maeyer, R.M. Verbeeck, M.G. Boltong, J. Ginebra, F.C. Driessens, J.A. Planell, Setting reaction and hardening of an apatitic calcium phosphate cement, J. Dent. Res. 76 (4) (1997) 905–912.
[29] A. Barba, A. Diez-Escudero, Y. Maazouz, K. Rappe, M. Espanol, E.B. Montufar, M. Bonany, J.M. Sadowska, J. Guillem-Marti, C. Ohman-Magi, C. Persson, M.C. Manzanares, J. Franch, M.P. Ginebra, Osteoinduction by foamed and 3D-printed calcium phosphate scaffolds: effect of nanostructure and pore architecture, ACS. Appl. Mater. Interfaces. 9 (48) (2017) 41722–41736.
[30] C. Kampleitner, J. Obi, N. Vassilev, M.M. Epstein, O. Hoffmann, Biological compatibility profile on biomaterials for bone regeneration, J. Vis. Exp. (141) (2018).
[31] A. Bernhardt, K. Koperski, M. Schumacher, M. Gelinsky, Relevance of osteoclast-specific enzyme activities in cell-based in vitro resorption assays, Eur. Cell Mater. 33 (2017) 28–42.
[32] J.P. Rissanen, M.I. Suominen, Z. Peng, J.M. Halleen, Secreted tartrate-resistant acid phosphatase 5b is a marker of osteoclast number in human osteoclast cultures and the rat ovariectomy model, Calcif. Tissue Int. 82 (2) (2008) 108–115.
[33] M.T. Rojewski, R. Lotfi, C. Gjerde, K. Mustafa, E. Veronesi, A.B. Ahmed, M. Wiesneth, S. Korper, L. Sensebe, P. Layrolle, S. Hellem, H. Schrezenmeier, Translation of a standardized manufacturing protocol for mesenchymal stromal cells: a systematic comparison of validation and manufacturing data, Cytotherapy. 21 (4) (2019) 468–482.
[34] M.A. Brennan, D.S. Monahan, B. Brulin, S. Gallinetti, P. Humbert, C. Tringides, C. Canal, M.P. Ginebra, P. Layrolle, Biomimetic versus sintered macroporous calcium phosphate scaffolds enhanced bone regeneration and human mesenchymal stromal cell engraftment in calvarial defects, Acta Biomater. 135 (2021) 689–704.
[35] P. Bankhead, M.B. Loughrey, J.A. Fernandez, Y. Dombrowski, D.G. McArt, P.D. Dunne, S. McQuaid, R.T. Gray, L.J. Murray, H.G. Coleman, J.A. James, M. Salto-Tellez, P.W. Hamilton, QuPath: Open source software for digital pathology image analysis, Sci. Rep. 7 (1) (2017) 16878.
[36] P. Humbert, M.A. Brennan, N. Davison, P. Rosset, V. Trichet, F. Blanchard, P. Layrolle, Immune modulation by transplanted calcium phosphate biomaterials and human mesenchymal stromal cells in bone regeneration, Front. Immunol. 10 (2019) 663.
[37] Y. Shiwaku, K. Tsuchiya, L. Xiao, O. Suzuki, Effect of calcium phosphate phases affecting the crosstalk between osteoblasts and osteoclasts in vitro, J. Biomed. Mater. Res. a 107 (5) (2019) 1001–1013.
[38] F. Barrere, C.A. van Blitterswijk, K. de Groot, Bone regeneration: molecular and cellular interactions with calcium phosphate ceramics, Int. J. Nanomedicine 1 (3) (2006) 317–332.
[39] J.M. Anderson, A. Rodriguez, D.T. Chang, Foreign body reaction to biomaterials, Semin. Immunol. 20 (2) (2008) 86–100.
[40] G.J. Ahmed, E. Tatsukawa, K. Morishita, Y. Shibata, F. Suehiro, M. Kamitakahara, T. Yokoi, T. Koji, M. Umeda, M. Nishimura, T. Ikeda, Regulation and biological significance of formation of osteoclasts and foreign body giant cells in an extraskeletal implantation model, Acta Histochem. Cytochem. 49 (3) (2016) 97–107.
[41] M.H. Mankani, S.A. Kuznetsov, P.G. Robey, Formation of hematopoietic territories and bone by transplanted human bone marrow stromal cells requires a critical cell density, Exp. Hematol. 35 (6) (2007) 995–1004.
[42] M. Mebarki, L. Coquelin, P. Layrolle, S. Battaglia, M. Tossou, P. Hernigou, H. Rouard, N. Chevallier, Enhanced human bone marrow mesenchymal stromal cell adhesion on scaffolds promotes cell survival and bone formation, Acta Biomater. 59 (2017) 94–107.
[43] P. Humbert, M.A. Brennan, J. De Lima, R. Brion, A. Adrait, C. Charrier, B. Brulin, V. Trichet, Y. Coute, F. Blanchard, P. Layrolle, Apoptotic mesenchymal stromal cells support osteoclastogenesis while inhibiting multinucleated giant cells formation in vitro, Sci. Rep. 11 (1) (2021) 12144.
[44] A. Galleu, Y. Riffo-Vasquez, C. Trento, C. Lomas, L. Dolcetti, T.S. Cheung, M. von Bonin, L. Barbieri, K. Halai, S. Ward, L. Weng, R. Chakraverty, G. Lombardi, F.M. Watt, K. Orchard, D.I. Marks, J. Apperley, M. Bornhauser, H. Walczak, C. Bennett, F. Dazzi, Apoptosis in mesenchymal stromal cells induces in vivo recipient-mediated immunomodulation, Sci. Transl. Med. 9 (416) (2017).
[45] Z. Nie, Z. Hu, X. Guo, Y. Xiao, X. Liu, J.D. de Bruijn, C. Bao, H. Yuan, Genesis of osteoclasts on calcium phosphate ceramics and their role in material-induced bone formation, Acta Biomater 157 (2023) 625–638, doi:10.1016/j.actbio.2022.11.005.
[46] D. Li, Y. Jiang, P. He, Y. Li, Y. Wu, W. Lei, N. Liu, J.D. de Bruijn, H. Zhang, H. Zhang, P. Ji, H. Yuan, M. Li, Hypoxia drives material-induced heterotopic bone formation by enhancing osteoclastogenesis via M2/lipid-loaded macrophage axis, Adv. Sci. (Weinh). 10 (15) (2023) e2207224, doi:10.1002/advs.202207224.
[47] X. Wang, Y. Yu, L. Ji, Geng Zhen, J. Wang, C. Liu, Calcium phosphate-based materials regulate osteoclast-mediated osseointegration, Bioact. Mater. 6 (12) (2021) 4517–4530, doi:10.1016/j.bioactmat.2021.05.003.
[48] N. Rana, S. Suliman, S. Mohamed-Ahmed, S. Gavasso, B.T. Gjertsen, K. Mustafa, Systemic and local innate immune responses to surgical co-transplantation of mesenchymal stromal cells and biphasic calcium phosphate for bone regeneration, Acta Biomater. 141 (2022) 440–453.